JOURNAL OF CATALYSIS 141, 219–238 (1993)

Two-Component Catalysts for Low-Temperature CO Oxidation: A Monte Carlo Study

R. K. HERZ,*,[1] A. BADLANI,* D. R. SCHRYER,† AND B. T. UPCHURCH†

*Chemical Engineering Group, Department of Applied Mechanics and Engineering Sciences, University of California, San Diego, California 92093-0310; and †NASA Langley Research Center, Hampton, Virginia 23681-0001

Received August 20, 1992; revised January 5, 1993

The reaction of CO and O_2 at low temperature over composite, noble-metal/reducible-oxide catalysts is simulated using Monte Carlo techniques. High activity for CO oxidation can be obtained over a composite material composed of a highly interspersed mixture of one type of site that adsorbs CO and O_2 and another type of site that adsorbs O_2 without significant CO inhibition. For example, the rate over Pd under 1% of an atmosphere of CO at room temperature is predicted to increase 10 orders-of-magnitude with addition of 1% of surface sites which adsorb O_2 but not CO. For most reaction rules and parameter values, a roughly 50–50 mixture of the two types of sites gives the greatest activity per unit total surface area. This result is determined by the reaction stoichiometry and the fact that the two reactants primarily adsorb separately on the two different types of sites. In a randomly distributed mixture, the two types of sites have widely differing activities which depend on the local site configurations. The local site configurations of the most active sites in a random surface are similar to site configurations found in a search for optimal configurations. The site configurations found in the search for optimal configurations were about 20% more active than the random surfaces of the same overall composition. This relatively small increase may be due to the simple steric requirements of CO and O_2 adsorption. We expect that similar searches for optimal site configurations will be more fruitful for reactions with more complex steric requirements.

INTRODUCTION

For most of us who are familiar with conventional CO oxidation catalysts which are active only at temperatures above about 150°C, observation of rapid CO oxidation at room temperature can be startling. In our laboratories, for example, we have measured, at room temperature, 56% conversion of a stoichiometrically balanced, atmospheric-pressure mixture of 1% CO and 0.5% O_2 in N_2 flowing at 1.2 cm^3/s over 0.2 g of Au/MnO_2 (*1*). Au/MnO_2 and related materials are some of the few heterogeneous catalysts with activities at ambient conditions which may approach those of biological catalysts. The objective of the work presented here is to help develop an understanding of how these heterogeneous catalysts are able to oxidize CO at ambient and subambient temperatures.

There are several applications in which the catalytic oxidation of CO near ambient temperature is desirable. One such application is removal of CO as a contaminant of breathing air in enclosed spaces such as submarines and space vehicles and in burning structures or mines (*2*). Another is oxidation of CO in automobile engine exhaust during cold starts (*3*). A third is regeneration of CO_2 in transversely excited atmospheric pressure (TEA) CO_2 lasers (*4*, *5*). Stoichiometrically balanced mixtures of CO and O_2 are generated during the operation of CO_2 TEA lasers through the decomposition of CO_2 by the electrical discharge that initiates the lasing process. Consumption of CO_2 and buildup of O_2 degrades the performance of

[1] To whom correspondence should be addressed.

0021-9517/93 $5.00

such a laser. A CO oxidation catalyst that operates under low-temperature conditions is desirable for the development of closed-cycle or sealed CO_2 TEA lasers, which have applications such as mapping of earth's wind patterns from space by laser Doppler anemometry and remote sensing of environmental pollutants by infrared spectrometry (*6*).

The reaction between CO and O_2 proceeds at a negligible rate over metal catalysts near ambient temperature, even though the reaction is thermodynamically favored and there are several metals, including Pt and Pd, which can chemisorb both species and, thus, should permit a Langmuir–Hinshelwood-type reaction mechanism to occur (*7*). The explanation frequently given for the lack of reaction under these superficially favorable conditions is that CO requires only a single vacant adsorption site and O_2 requires two adjacent vacant sites, so that a clean surface exposed to a mixture of CO and O_2 quickly becomes covered with CO, which prevents O_2 adsorption, except at low CO-to-O_2 ratios (*8*). Only at elevated temperatures, where CO desorption becomes significant, do enough adjacent adsorption-site pairs become available to allow significant O_2 chemisorption and reaction to occur.

A demonstration of the foregoing explanation was presented by Ziff *et al.* (*8*). Using a simple stochastic (Monte Carlo) model which assumed equal sticking probabilities for CO and O_2 and neglected CO desorption, they showed that chemisorption and reaction of both CO and O_2 could occur on a uniform surface only when the ratio of the partial pressures of CO to O_2, P_{CO}/P_{O_2}, fell between 0.59 and 1.0. At higher P_{CO}/P_{O_2}, including the stoichiometrically balanced case where $P_{CO}/P_{O_2} = 2$, the surface becomes covered with CO. If the sticking probability of CO is greater than that of O_2, which would be the case for a Pt surface, these partial-pressure ratios would be shifted downward and further away from stoichiometry.

The treatment by Ziff *et al.* is quite general and should apply to any single-component catalyst in which a species requiring only a single adsorption site is to be oxidized by O_2. A number of other workers have studied the CO + O_2 reaction, or the general A + B_2 reaction, over surfaces using Monte Carlo (*9–18*) and cellular automaton simulations (*19*). Ertl and co-workers have used cellular automaton simulations to study the participation of Pt surface reconstruction in rate oscillations during CO oxidation (*20, 21*). Related Monte Carlo studies have been made of the general A + B reaction over surfaces (*22–30*). Monte Carlo simulations are required in order to study the kinetics of surface reactions in which adsorbed species are not randomly distributed over the surface; traditional kinetic models using algebraic rate equations assume such random distribution.

The fact that a CO oxidation catalyst must perform two distinct functions, adsorption of CO and dissociative adsorption of O_2, suggests that a "composite material" composed of an intimate mixture of two different materials, each with optimal properties for one of the two catalytic functions required, would have significant low-temperature activity (*31*). In such an ideal "composite catalyst," CO and O_2 would not compete for the same adsorption sites and, thus, CO inhibition of low-temperature CO oxidation would be eliminated.

A class of composite materials is currently under development for application as low-temperature CO oxidation catalysts in CO_2 TEA lasers and in breathing air purification. We have given the term "noble-metal/reducible-oxide" (NMRO) catalysts to this class of catalytic materials (*32*). Examples include Au/MnO_2 (*33*), Au/Fe_2O_3 (*34*), and Pd/SnO_2 (*35, 36*). These materials have greater activity and stability than the conventional low-temperature CO oxidation catalyst, Hopcalite, which is a mixture of Cu and Mn oxides with small quantities of other oxides (*37*). In each of the NMRO catalysts, neither of the separate compo-

nents have appreciable activity for CO oxidation at low temperature and, thus, a synergistic interaction is present in the two-component materials. Although the mechanisms of CO oxidation over these materials are not known in detail (*32*), a probable general explanation for their low-temperature activity is that the noble metal chemisorbs CO and the reducible oxide provides sites that dissociatively adsorb O_2. There are also indications that surface hydrogen or hydroxyl participates in the dissociative adsorption of O_2 and the oxidation of adsorbed CO at low temperature (*38*).

One barrier to our understanding of the mechanism of CO oxidation over these composite catalysts is that we do not know the surface structure and composition of these materials. Discrete noble-metal particles are present in many catalyst formulations. Recently, Brosilow *et al.* (*9*) adapted the model of Ziff *et al.* (*8*) to investigate the effect of a reducible-oxide support on the oxidation of CO over noble-metal particles. The effect of the reducible-oxide support was simulated by holding the coverage of adsorbed oxygen at saturation at the perimeter of noble metal particles. Near a stoichiometric ratio of CO and O_2, $P_{CO}/P_{O_2} = 2.1$, the reaction rate was nonzero for a distance of three or four noble-metal lattice sites with penetration from the perimeter into the noble-metal particle; the rate would be zero everywhere on the particle in the absence of the reducible oxide at the perimeter. At lower CO to O_2 ratios, the effect of the reducible oxide penetrates further into the noble-metal particle. These results suggest that very small noble-metal particles would provide the highest rate per noble-metal surface atom, especially for stoichiometric mixtures.

Enhanced reaction at the perimeter of noble metal particles in contact with a reducible-oxide support is not the only possible reason for the enhanced activity of NMRO catalysts. The activity of Pt/SnO_2 is increased by reducing pretreatments, and Hoflund and co-workers (*39*, *40*) reported that such pretreatment leads to the formation of Pt–O–Sn, $Pt(OH)_2$, metallic Pt and Sn, and Pt–Sn alloy. In related work, Oh and Carpenter (*41*) found that a Pt–Rh catalyst which contained bimetallic Pt–Rh particles had enhanced activity for CO oxidation. They proposed that Rh provided sites favorable for O_2 adsorption near CO adsorbed on Pt. Rh may have been present as a reducible oxide in the Pt–Rh bimetallic particles, making this catalyst a member of the NMRO class of materials. Logan and Paffett (*42*) studied the CO oxidation activity of a 50–50 Pd–Sn surface alloy. They found that Pd–Sn had higher activity than pure Pd but also found that the Sn oxidized to form a partial SnO_x overlayer. Work with Rh/TiO_2 has demonstrated that the unique activity of this material after high temperature reduction pretreatment is related to the presence of TiO_x overlayers covering much of the surface of the Rh particles (*43*, *44*). Although the unique activity in these cases may result from reaction at the interface between the noble-metal and oxide overlayers, this inferface may be complex and the noble-metal and reducible-oxide components highly interspersed.

In this work we investigate the reaction of stoichiometric mixtures of CO and O_2 over highly interspersed mixtures of noble-metal and reducible-oxide sites using Monte Carlo simulations. We demonstrate that a two-component catalyst, in which one component chemisorbs CO and the second component chemisorbs O_2 but does not significantly chemisorb CO, makes possible the low-temperature reaction of stoichiometric mixtures of CO and O_2. We suggest that this feature accounts for the pronounced low-temperature activity of NMRO catalysts which readily catalyze the reaction of stoichiometric mixtures of CO and O_2 at room temperature and below (*4*, *34*). Monte Carlo simulations are performed in order to investigate the effects of different O_2 adsorption rules, the effect of changing the O_2 adsorption probability, the kinetic orders of the reaction, and the effects of changing the CO

desorption probability. Finally, a search is made for optimal configurations of surface sites as a first step towards the rational design of composite catalysts. With the exceptions of the study of uniform surfaces with heterogeneous boundaries by Brosilow *et al.* (*9*) and the study of uniform surfaces with defects by Vlachos *et al.* (*15, 45*), this is the first Monte Carlo study, of which we are aware, of catalytic reaction over nonuniform, multicomponent surfaces.

REACTION MODEL

Noble-metal sites which adsorb CO are referred to in this work as α sites and the reducible-oxide sites which adsorb O_2 are referred to as β sites. Previous Monte Carlo simulation work on uniform surfaces has referred to the CO + O_2 reaction as a member of a general class represented by the reaction A + B_2. The labels α and β have been used previously to distinguish between different sites on catalyst surfaces identified during thermal desorption experiments (*46*). Thus, the cases studied here can be referred to as examples of the general A + B_2 reaction over a two-component, α–β surface.

The identity of individual β sites is not specified in the Monte Carlo simulations. In Pt/SnO_2, for example, actual individual β sites might consist of one or more of the following: $(Sn)_z$, $(SnH_y)_z$, $(SnO_x)_z$, $(SnO_xOH_y)_z$, $(SnO_xH_y)_z$, $(SnOH_y)_z$, etc. Interspersion of noble-metal and reducible-oxide materials should lead to modification of the properties of each material. Such modifications are not explicitly considered here, although they could be studied by determining the effect of varying the adsorption, desorption and reaction probabilities assigned to each site. Rather, these simulations mainly probe geometric effects such as the effects of changing the relative positions of the two sites in a surface.

The main loop in the simulation program is shown in Fig. 1. This program was developed in order to consider sets of parameter values where adsorption and reaction probability values are within several orders-of-magnitude of each other. The adsorption, desorption, and reaction probabilities are independent of surface coverage. The O_2 sticking probability is the same for all allowed site pairs, and the reaction probability is the same whether the O atom is adsorbed on an α site or a β site. Surface diffusion is not described. A lattice of square sites was used in all simulations.

The following "base set" of parameter values was used below, except where specified otherwise:

(a) CO sticking probability (probability that a gas phase CO molecule striking a vacant α site will adsorb): $p_1 = 1$;

(b) O_2 sticking probability (probability that a gas phase O_2 molecule striking a vacant pair of sites that correspond to the specified set of O_2 adsorption rules—e.g., α–α, α–β,β–β—will adsorb): $p_2 = 1$;

(c) CO desorption probability (probability that a CO molecule will desorb when a site is selected randomly at a frequency equal to the CO collision frequency and the site is occupied by an adsorbed CO; as defined, this probability is inversely proportional to CO pressure): $p_3 = 0$;

(d) reaction probability (probability that a reaction event will occur when a pair of neighboring sites is selected randomly and the site pair is occupied by one adsorbed CO molecule and one adsorbed O atom): $p_4 = 0.4$;

(e) actions allowed on diagonally adjacent pairs of sites,

(f) stoichiometrically balanced ratio of gas-phase CO and O_2: $P_{CO}/P_{O_2} = 2$.

The differing molecular weights of CO and O_2 were taken into account when determining the relative collision frequencies of these reactants in the simulations.

Reaction rates are reported relative to the CO collision frequency. The results presented here are expected to correspond most closely to reaction over Pt/SnO_2 and Pd/SnO_2 catalysts at room temperature, where the CO sticking probability is near one and the CO desorption probability is near zero. The results presented also apply

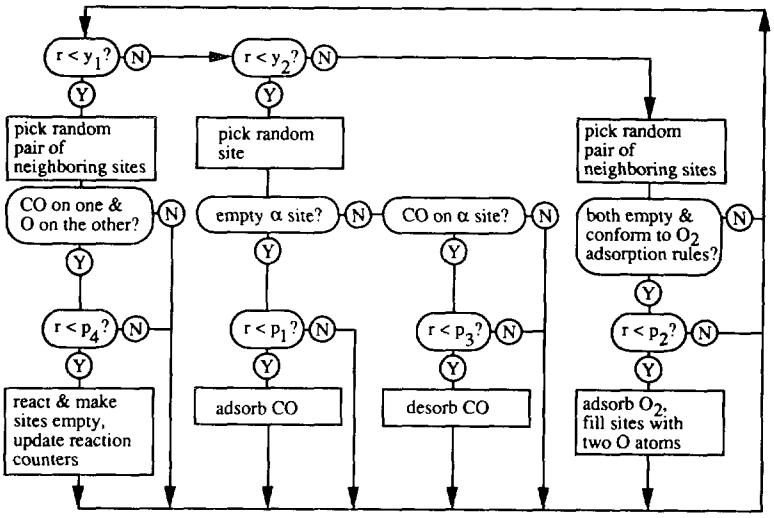

FIG. 1. Main loop in the Monte Carlo simulations. r = new random number between 0 and 1 generated at each step within the loop. y_1 = fraction of iterations that are checks for reaction = $y_2 (P_{CO,base}/P_{CO})/[1 + y_2 (P_{CO,base}/P_{CO})]$, where $(P_{CO,base}/P_{CO})$ is the ratio of the CO partial pressure for the base set of conditions to the CO partial pressure for the specific simulation run. y_1 is defined such that the frequency of checks for reaction in the program at the base set of conditions equals the frequency of CO collisions and such that the frequency of checks for reaction in "real time" is independent of CO pressure. y_2 = fraction of gas molecules colliding with the surface that are CO molecules. p_1 = CO sticking probability. p_2 = O_2 sticking probability. p_3 = CO desorption probability. p_4 = reaction probability. See text for further explanation of probabilities.

to CO sticking probabilities less than one when the other probabilities and the reaction rate are normalized properly with respect to the CO sticking probability. Here, we refer to the unnormalized probabilities and rates for simplicity.

All simulations were performed starting from a clean surface and run to steady-state conditions. In most cases, steady state was reached within 1000 Monte Carlo steps, where, in one Monte Carlo step, the loop in Fig. 1 is repeated the number of times equal to the total number of sites in the array. Cases which did not reach steady state within about 1000 Monte Carlo steps eventually deactivated completely. All reaction rates reported are average steady-state rates. In most cases, these rates were obtained by starting averaging after attainment of steady state at 3600 Monte Carlo steps into the run and averaging over the subsequent 3900 Monte Carlo steps.

For the parameter values used here, the effect of β sites on α sites is localized and propagates only a short distance into a "patch" or "particle" of α sites. Figure 2 shows the variation in reaction rate on α

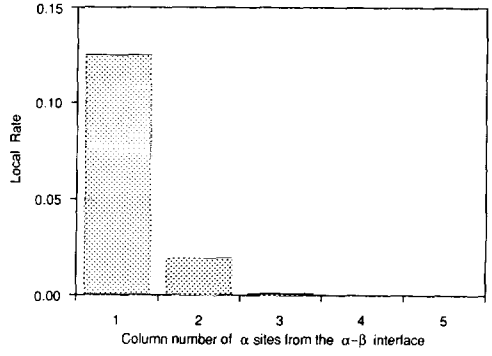

FIG. 2. Local rate vs distance from a semi-infinite linear α–β interface. The local rate is equal to the number of reaction events on an α site per CO collision with that site.

sites with distance from a semi-infinite α–β interface for the base set of parameters and for a case in which O_2 can adsorb on any pair of neighboring sites. The reaction rate is zero everywhere except for the three columns or rows of α sites nearest the α–β interface. This result is similar to that obtained by Brosilow *et al.* (*9*) at P_{CO}/P_{O_2} = 2.1 for adsorption-limited reaction.

RANDOM α–β SITE DISTRIBUTIONS

A 42 × 26 lattice with 1092 total sites and periodic boundaries was used for the simulations of all-α and random α–β surfaces. Random α–β surfaces represent the opposite extreme in geometric α–β configuration from the noble-metal particles on reducible-oxide supports simulated by Brosilow *et al.* (*9*). Some Pt–Sn surface alloys have a highly interspersed geometry (*42*); reaction over other Pt–Sn alloys may involve an intermediate α–β geometry, which might be obtained in simulations by "annealing" initially random surfaces.

For the case in which O_2 can adsorb on any site pair and the CO desorption probability is zero, the reaction rate for the all-α surface is zero. The rate is nonzero for the all-α surface for nonzero CO desorption probabilities. For low CO desorption probabilities, the rate increases dramatically when β sites are added to the surface. The relative increase is inversely related to the CO desorption probability. At ambient temperature over Pd, the CO desorption frequency from a site is on the order of 10^0 s^{-1} (*7*). This desorption frequency leads to a CO desorption probability, as defined above, of 10^{-7} at P_{CO} = 0.01 atm, a CO pressure characteristic of CO_2 TEA lasers (*4*). With this value of the CO desorption probability, the overall rate increases by 10 orders-of-magnitude—from 10^{-14} reaction events per CO collision with the surface to 10^{-4}—as the fraction of β sites is increased from 0 to 1%. This result demonstrates the extreme sensitivity of steady-state CO oxidation rates over Pd and Pt to the addition of small amounts of an oxygen adsorbing component that is not inhibited by CO. In an experimental demonstration of a related phenomenon, Mundshau and Rausenberger (*47*) used photoelectron microscopy to show the presence of defect sites present in low concentration in the surface of single crystal Pt that adsorb CO only weakly and initiate the transient burn-off of inhibiting CO overlayers by O_2.

A CO desorption probability of zero was used in most of this work in order to simulate the strong CO adsorption on noble metal sites at ambient temperatures and, thus, the strong inhibition of O_2 adsorption on Pt-group noble metals. In general, the absence of reactant desorption and surface diffusion in Monte Carlo simulations produces results which highlight the geometric effects present in the physical system modeled.

The reaction rate is zero for all α-plus-β surfaces with no CO desorption when O_2 adsorption is not allowed on β–β pairs. This is because all α sites are saturated with CO in this case, thus blocking O_2 adsorption on α–α and α–β pairs. The rate is nonzero with no CO desorption on α-plus-β surfaces when oxygen adsorption is allowed on β–β pairs.

We focus on the two cases of adsorption of O_2 on (a) any site pair and (b) only β–β site pairs. In each of these two cases, the O_2 sticking probability is the same on all allowed site pairs. In real catalysts, we would expect that the sticking probability would be different on different site pairs. The two cases considered here are limiting cases, with real systems possibly having behavior intermediate between these two cases.

Figure 3 shows the steady-state rate-per-α-site vs the fraction of β sites present in the surface ("fraction-β" below). The rate-per-α-site is equal to the average number of reaction events per CO collision with an α site. In many cases, the noble metal component represented by the α sites may be the major cost factor in a catalyst. The open circles are for the case in which O_2 can adsorb on any site pair. The solid diamonds are for the case which O_2 can only adsorb

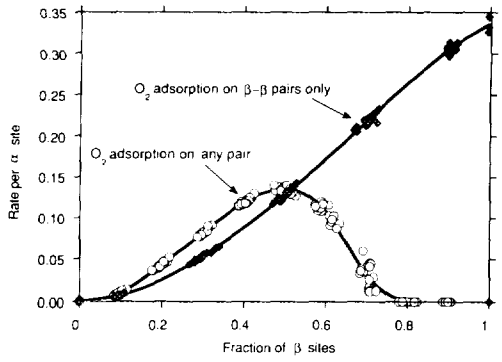

FIG. 3. Steady-state rate-per-α-site vs fraction-β for the base set of parameters. The rate-per-α-site is equal to the average number of reaction events per CO collision with an α site.

on β–β pairs. At each nominal fraction-β, 20 runs were performed to show the variation in rate from run to run, except for only three runs at fraction-β = 0.99 for the solid diamonds. At each specific fraction-β, the variation in rate is caused by the fact that different random configurations of α and β sites have somewhat different activities.

For the case in which O_2 adsorption is allowed on β–β pairs only, the rate-per-α-site is zero at fraction-β = 0, since no O_2 can adsorb, and increases continuously as the fraction of β sites is increased. The rate-per-α-site is somewhat more linear than simply being proportional to the square of the fraction of β sites. The rate-per-α-site approaches a value of 0.33 reaction events per CO collision with an α site as the fraction of β sites approaches one, that is, in the limit of isolated α sites surrounded by β sites. In surfaces with high fraction-β but before this limit, two widely separated α sites are more active than two adjoining α sites but are less active than two α sites separated by a distance of one or two β sites. In the latter case, O_2 adsorption and reaction are enhanced in the region between the two α sites since there is an increased rate of formation of vacant β–β site pairs in this region.

For the case in which O_2 adsorption is allowed on any site pair, the rate-per-α-site goes through a maximum at fraction-β = 0.5. To the left of the rate maximum, the rate increases as more β sites are added to the surface because O_2 can adsorb on β sites next to CO molecules adsorbed on α sites. To the right of the rate maximum, the rate-per-α-site decreases as more β sites are added to the surface. This occurs because α sites are becoming increasingly dispersed among β sites and, thus, are becoming more susceptible to deactivation by irreversibly adsorbed oxygen atoms. These oxygen atoms cannot desorb because the oxygen desorption probability is zero. They cannot be removed by reaction because there are no neighboring α sites in the local vicinity which are not also deactivated by oxygen.

Figure 4 shows a "snapshot" of the surface for the two cases at fraction-β = 0.5. The reaction rates are approximately equal for both cases at this fraction-β. Note that there is less CO present on the surface for the case where O_2 can adsorb on any site pair. This is because some α sites are covered with adsorbed oxygen atoms. Relatively isolated α sites are deactivated by this adsorbed oxygen. Oxygen adsorbed on α sites near other α sites covered with CO can be removed by reaction. At fraction-β = 0.5, the deactivation of isolated α sites by oxygen roughly balances the contribution to reaction by oxygen adsorption on α sites which remain active. Qualitatively, adsorbed CO and O are interspersed for the case where O_2 can adsorb only on β–β pairs, whereas adsorbed CO and O are found primarily in separate patches for the case where O_2 can adsorb on any site pair as a result of the coverage and deactivation of isolated α sites by adsorbed O.

For the case in which O_2 adsorption is allowed only on neighboring β–β pairs, isolated β sites are inactive, of course. Isolated β sites are also inactive for the case in which O_2 adsorption is allowed on any site pair when the CO desorption probability is zero. With a nonzero CO desorption probability for this second case, an isolated β site is

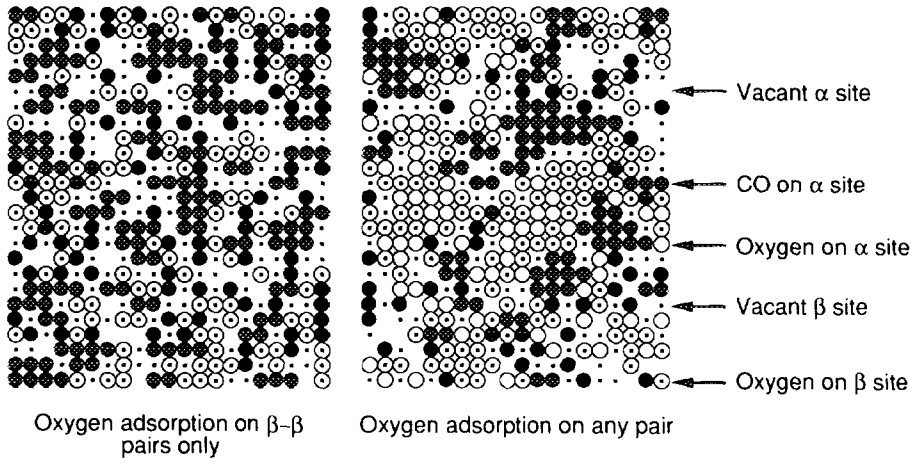

FIG. 4. Instantaneous surface configurations during steady-state reaction for two cases of O_2 adsorption. The fraction of β sites is 0.5 for both cases and the base set of parameters is used. Only parts of the complete surfaces are shown.

active but has a much lower activity than a pair of neighboring β sites. An isolated *pair* of β sites is active for both cases (O_2 adsorption only on β–β pairs, O_2 adsorption on any pair) with no CO desorption. Such an isolated β–β pair, however, is more active for the case in which O_2 can adsorb on any site pair since O_2 adsorption can involve a neighboring α site and one of the β sites, not just the β–β pair itself. The height of the solid curve above the dashed curve at low fraction-β shows the extent to which O_2 adsorption on α–α and α–β pairs contributes to the reaction rate for the case in which O_2 adsorption can occur on any site pair. The differences between these two cases decrease as the oxygen sticking probability decreases.

For the case in which O_2 adsorption is allowed on any site pair, note in Fig. 3 that the scatter of rates at a given fraction-β is higher at large fraction-β than at low fraction-β. This scatter at large fraction-β is caused by the fact that different proportions of site configurations susceptible to oxygen poisoning are generated at the start of the different runs. The surface becomes completely oxygen poisoned for a fraction of β sites equal to 0.8 and above. The time required for complete deactivation to occur in these cases is much longer than the normal start-up transient for runs in which the surface remains active.

For the runs shown in Fig. 3, actions involving diagonally adjacent sites are allowed. When "diagonal actions" involving these "diagonal pairs" are not allowed, the reaction rate decreases by about one-third. However, when diagonal actions are not allowed there is no qualitative change in behavior, with one exception: for the case in which O_2 can only adsorb on β–β pairs, the rate-per-α-site drops to zero as the fraction of β sites approaches one rather than approaching a nonzero value. That is, individual α sites surrounded by β sites are inactive at steady state when diagonal actions are not allowed. After an initial transient in which CO adsorbs on these sites and reacts with oxygen atoms which have adsorbed on neighboring β sites, the reaction ceases. This is because oxygen is removed by reaction from the β sites to the left and right and top and bottom of an α site and this oxygen cannot be replaced. Since, at steady state, the β sites neighboring the α site diagonally, and essentially all other β sites, are filled with oxygen atoms, these vacant β sites to

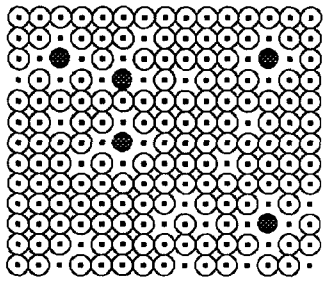

FIG. 5. Instantaneous surface configuration during steady-state reaction for a case in which O_2 can adsorb on β–β pairs only; the fraction of β sites on the entire surface is 0.99, and the base set of parameters is used except that actions involving diagonally adjacent pairs of sites are not allowed. All α sites shown are covered by adsorbed CO, as indicated by the large black circles. The α site located in the upper left and the two α sites located on the far right are inactive because O_2 cannot adsorb on the vacant β sites (small black dots) located to their top and bottom and left and right. The two α sites located just left of center are active since O_2 can adsorb and react on the pair of β sites directly between them.

the left and right and top and bottom do not have any vacant adajcent β sites with which to form a vacant β–β pair to allow further O_2 adsorption. This inactive steady-state site configuration is shown in Fig. 5.

Figure 6 shows the same runs plotted in Fig. 3 but now plotted as the "overall rate" vs fraction-β. The overall rate is defined as the average number of reaction events per CO collision with any site on the surface. This overall rate corresponds to the rate that would be measured in the laboratory in moles per time per unit BET surface area. Note that both cases show a maximum in overall rate vs fraction-β. Although the rate-per-α-site is highest at high fraction-β for the case in which O_2 adsorbs only on β–β pairs, the overall rate is relatively low because of the low fraction of α sites. For both cases at low fraction-β (0 to 0.3), the overall reaction rate in each case is roughly proportional to the fraction of α sites times the square of the fraction of β sites. The overall rate for the case in which O_2 adsorbs only on β–β pairs continues to be roughly described by this proportionality from low to high fraction-β.

The results shown in Fig. 6 are in qualitative agreement with the experimental results of Upchurch *et al.* (*48*). They found that the CO oxidation activity, per unit weight, of a series of Pt/SnO_2 catalysts was highest at intermediate Pt–SnO_2 weight ratios. Surface composition measurements, especially at low noble-metal surface fractions, will be required in future studies in order to distinguish between different O_2 adsorption rules.

Alternate Rules for O_2 Adsorption

Two different sets of rules for O_2 adsorption were discussed above: O_2 adsorption on any site pair and O_2 adsorption only on β–β pairs. The comparison between these two sets of rules demonstrates that, whenever O_2 can adsorb on β–β pairs, the predominate mode of reaction involves O_2 adsorption on these pairs, with reaction involving O_2 adsorption on α–β and, especially, α–α pairs contributing only slightly. The main contribution seen from allowing O_2 adsorption to involve α sites was to allow for oxygen poisoning of highly dispersed α sites at high fraction-β.

We have also investigated the behavior

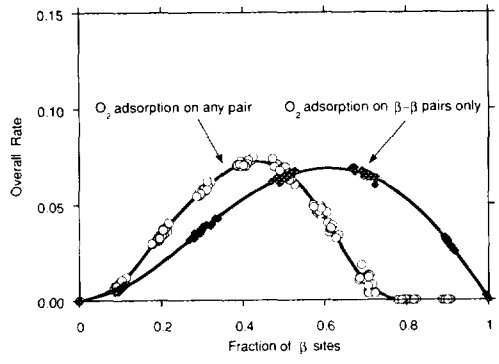

FIG. 6. The same runs in Fig. 3, now plotted as the overall rate vs fraction-β. The overall rate shown here is equal to the average number of reaction events per CO collision with any site on the surface. This rate would be proportional to the observed rate per total, or BET, surface area measured experimentally over an actual catalyst.

with other sets of site pairs on which O_2 adsorption is allowed. The case in which O_2 adsorption is allowed on α–β and β–β pairs behaves similarly to the case in which O_2 adsorption is allowed on all site pairs.

Two sets of rules were investigated which do not allow O_2 adsorption on β–β site pairs: O_2 adsorption only on (a) α–β pairs and (b) α–α and α–β pairs. For these sets of rules, the surfaces are inactive when the CO desorption probability is zero, since all α sites are covered by CO, preventing O_2 adsorption. As the CO desorption probability is increased slightly (e.g., to 0.01) from zero, the reaction rate becomes nonzero at most fractions of β sites. With a nonzero CO desorption probability, the rate-per-α-site goes through a maximum at intermediate fraction-β. The rate remains low at low fraction-β because of CO poisoning of the α sites in α–α and α–β site pairs. In many cases, the rate remains zero at high fraction-β because of oxygen poisoning of α sites. Specifically, for O_2 adsorption on α–β pairs only and for a CO desorption probability of 0.01, the rate remains zero at fraction-β = 0.7 and 0.9 for diagonal actions not allowed but is nonzero at these fraction-β when diagonal actions are allowed. For O_2 adsorption on α–α and α–β pairs only and for a CO desorption probability of 0.01, the rate is zero at fraction-β = 0.9 whether or not diagonal actions are allowed. The effect of allowing diagonal actions is to enhance the reaction rate somewhat, except in the case mentioned above for O_2 adsorption on α–β pairs only where inactive surfaces become active if diagonal actions are allowed.

Variation of O_2 Sticking Probability

In the simulations presented above, the O_2 sticking probability was set equal to the CO sticking probability, as in the Monte Carlo models of Ziff and co-workers (*8, 49*). Over noble metals, O_2 sticking probabilities are lower than CO sticking probabilities (*50*). Here, the effect of reducing the O_2 sticking probability is investigated for cases in which diagonal actions are allowed.

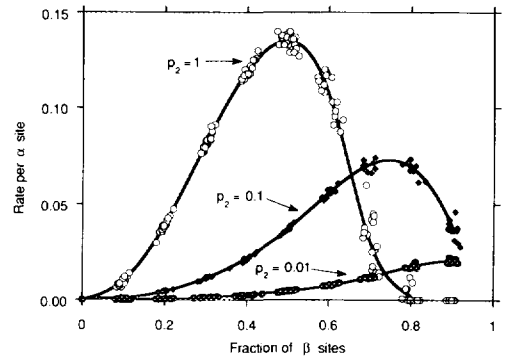

FIG. 7. Variation of O_2 sticking probability, p_2. O_2 can adsorb on any site pair and the base set of parameters was used except for the variation in p_2. Note that, as p_2 decreases, the shape of the curve for this case approaches the shape of the curve in Fig. 3 for the case in which O_2 can adsorb on β–β pairs only.

For the case in which O_2 adsorption is allowed only on β–β site pairs, decreasing the O_2 sticking probability decreases the rate at all fraction-β. For the case in which O_2 adsorption is allowed on any site pair, decreasing the O_2 sticking probability decreases the rate at low fraction-β because of the reduced rate of O_2 adsorption on all site pairs. This behavior is shown in Fig. 7. Decreasing the O_2 sticking probability increases the rate at high fraction-β because oxygen poisoning of highly dispersed α sites is reduced. The surface at fraction β = 0.8 goes from inactive to active when the O_2 sticking probability is decreased from 1.0 to 0.5. As a result of this behavior, the rate maximum shifts to higher fraction-β and reduces in amplitude as the O_2 sticking probability is decreased. The overall result is that, as the O_2 sticking probability is reduced to lower values, the case in which O_2 adsorption is allowed on any site pair exhibits behavior more similar to the case in which O_2 adsorption is allowed only on β–β pairs.

Apparent Orders of Reaction

The dependence of the reaction rate on changes in reactant pressure over small

ranges in reactant pressure can be reported in terms of a power-law rate expression. When the CO and O_2 pressures are varied independently, the rate can be expressed as $r = kP_{CO}^{\phi}P_{O_2}^{\gamma}$. This rate expression is an empirical correlation of results and does not represent a kinetic mechanism, and the reaction orders are not restricted to integer values. For the Monte Carlo results presented here, the apparent order of the reaction with respect to CO was determined by doubling the CO pressure, keeping the O_2 pressure constant and then using the equation

$$\phi = \frac{\ln(r_2/r_1)}{\ln 2}, \qquad (1)$$

where ϕ is the apparent order with respect to CO, r_1 is the rate (number of reaction events per unit "real time") at the base CO and O_2 pressures in a stoichiometrically balanced ratio, and r_2 is the rate obtained when the CO pressure was doubled. The apparent order with respect to O_2, γ, was determined in a similar manner by doubling the O_2 pressure and holding the CO pressure constant.

For a stoichiometrically balanced mixture of CO and O_2, the rate can be expressed as $r = kP_{CO}^{\eta} = k'P_{O_2}^{\eta}$, where $P_{CO} = 0.5P_{O_2}$ and where η is the apparent overall order. For the Monte Carlo results presented here, the apparent overall order of the reaction was determined by doubling both the CO and O_2 pressures while keeping the reactant pressure ratio stoichiometrically balanced. The overall order was then determined from the equation

$$\eta = \frac{\ln(r_2/r_1)}{\ln 2}, \qquad (2)$$

where r_1 is the rate at the base CO and O_2 pressures in a stoichiometrically balanced mixture, and r_2 is the rate obtained when both the CO and O_2 pressures are doubled. The overall order for a stoichiometric mixture will equal the sum of the individual orders, $\eta = \phi + \gamma$, when the overall and individual orders are determined for infinitesimally small variations in CO and O_2 pressures, or when the true kinetics obey the power-law expression exactly.

There are only a limited number of experimental studies that report the kinetics of the CO oxidation reaction at low temperature over NMRO catalysts. Although these studies have not provided a clear picture of the dependence of rate on reactant pressure, all show that the kinetics are different than those observed over single-component noble-metal catalysts. Stark and Harris (*4*) determined that the overall order of the reaction was approximately one for stoichiometrically balanced mixtures over Pd/SnO_2 and Pt/SnO_2, and Badlani (*1*) obtained the same result over Au/MnO_2. Over Pd/SnO_2 at low temperature, Bond *et al.* (*35*) found that the reaction was slightly negative order in CO. They also found that the reaction was approximately half order in O_2 over a range of O_2 concentration which depended on Pd concentration and temperature and tended to zero order at high O_2 concentrations. Sampson and Gudde (*51*) studied stoichiometric mixtures of CO and O_2 over a "precious metal"–SnO_2 catalyst at low temperature and found that the reaction was zero order in CO and first order in O_2. Logan and Paffett (*42*) determined that the reaction was slightly positive order in both CO and O_2 over a 50–50 Pd–Sn surface alloy.

Figure 8 shows the apparent reaction orders vs fraction-β for the Monte Carlo simulation case in which O_2 can adsorb on any site pair and for the base set of parameters. One interesting observation is that the overall order for the stoichiometric mixture is roughly constant and equal to 0.5 over most of the range of surface composition. Although the separate orders with respect to CO and O_2 change substantially over this range, these changes compensate each other. At small fraction-β, reaction orders are similar to those that would be observed over a noble metal: the rate is positive order in O_2 and negative order in CO due to CO inhibition of O_2 adsorption on α sites. At

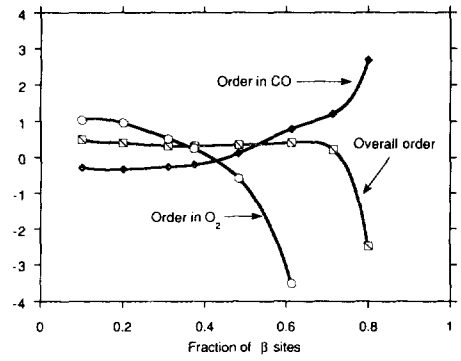

FIG. 8. Reaction orders vs fraction-β for the case in which O_2 can adsorb on any site pair and for the base set of parameters.

large fraction-β, the apparent orders are determined primarily by changes in oxygen poisoning of relatively isolated α sites: as the O_2 pressure increases the poisoning becomes more severe and the rate decreases; as the CO pressure increases α sites become more resistant to oxygen poisoning and the rate increases.

Figure 9 shows how the overall order varies with the O_2 sticking probability. When the O_2 sticking probability is 0.01, the overall order is approximately one, in agreement with most experimental measurements of reaction of stoichiometric mixtures over NMRO catalysts at low temperature (*1*, *4*, *51*), and the reaction is first order in O_2 and zero order in CO, in agreement with the experiments of Sampson and Gudde (*51*). Figure 10 shows a characteristic configuration of a surface with 90% β sites and an O_2 sticking probability of 0.01. At any given time during steady state, the α sites are nearly saturated with CO molecules, β sites neighboring α sites are nearly vacant, β sites far from α sites are saturated with oxygen. These results predict that the reaction rate is limited by the adsorption of O_2 at (or reoxidation of) reducible oxide sites located at the interface between the noble metal and reducible oxide components.

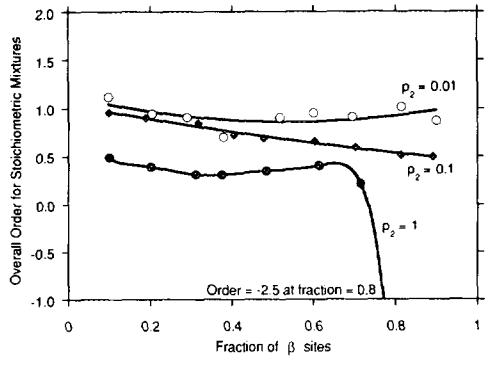

FIG. 9. Effect of varying the O_2 sticking probability, p_2, on the overall order for the case in which O_2 can adsorb on any site pair and for base set of parameters.

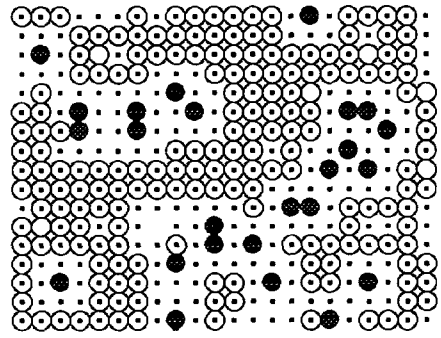

FIG. 10. Instantaneous surface configuration during steady-state reaction for the case in which O_2 can adsorb on any site pair; the fraction of β sites on the entire surface is 0.9, and the base set of parameters is used except that the O_2 adsorption probability, p_2, equals 0.01.

Figure 11 shows the overall order vs fraction-β for the case in which O_2 can adsorb only on β–β pairs and for the base set of parameters. Since there is no CO inhibition or oxygen poisoning in this case, the order in CO decreases toward zero and the order in O_2 and the overall order increase toward one as the O_2 sticking probability decreases. At low O_2 sticking probability, the behavior for the two cases of O_2 adsorption rules is similar since O_2 adsorption on α–α and α–β pairs becomes insignificant for the case in which O_2 can adsorb on any site pair.

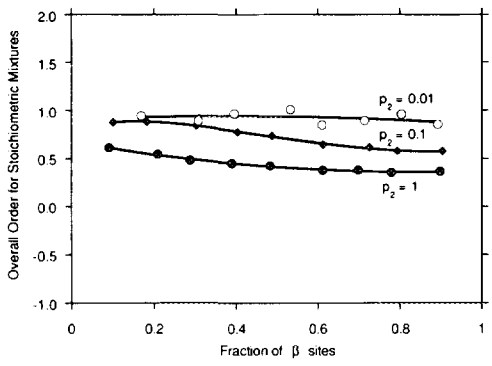

FIG. 11. Effect of varying the O_2 sticking probability, p_2, on the overall order for the case in which O_2 can adsorb only on β–β pairs and for the base set of parameters.

Variation of CO Desorption Probability

Over metal catalysts where CO inhibition dominates at low temperature, CO desorption is a critical kinetic step in determining the rate. CO desorption is also the most highly activated step in the mechanism of CO oxidation over metals (*7*). At relatively high P_{CO}/P_{O_2}, where the reaction is negative order in CO pressure, the overall reaction rate increases with temperature primarily as a result of an increased rate of CO desorption and a lower inhibiting CO coverage. Thus, apparent activation energies of the overall reaction (*42*) are in the same range, 80–120 kJ/mol, as the activation energy for CO desorption (*7*).

CO desorption is less critical over NMRO catalysts than over metals because CO inhibition is less important. Over these NMRO catalysts at relatively high P_{CO}/P_{O_2}, CO oxidation is only slightly positive (*42*) or slightly negative order in CO (*35*) and the apparent activation energies are substantially lower—roughly 20–40 kJ/mol (*1*, *42*)—than for metal catalysts.

The effect of increasing the CO desorption probability from zero was investigated with the Monte Carlo model for cases in which diagonal actions are allowed. For the case in which O_2 adsorption is allowed only on β–β site pairs, changing the CO desorption probability from zero to 0.01 produced only a slight decrease in rate at all fraction-β. Increasing the CO desorption probability further simply results in further decreases in reaction rate at all fraction-β.

For the case in which O_2 adsorption is allowed on any site pair, changing the CO desorption probability slightly from zero to 0.01 causes the all-α surface to become active but results in only slight changes in rate at higher fraction-β. As the CO desorption probability increases, the rate at low fraction-β increases and the rate at high fraction-β decreases such that the rate maximum shifts to lower fraction-β. This trend of a shift of the rate maximum to lower fraction-β continues as the CO desorption probability is further increased, as shown in Fig. 12.

Continuing with the cases shown in Fig. 12, for a CO desorption probability of 0.3, the surface at fraction-β = 0.7 has become inactive as more α sites become susceptible to oxygen poisoning as the CO coverage on these sites decreases with the increase in CO desorption rate. Except for cases such as this in which a surface becomes completely and irreversibly deactivated, the change in rate over a given surface with increase in CO desorption probability is reversible when the CO desorption probability is later decreased.

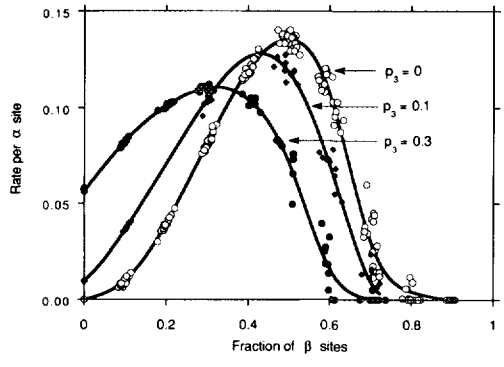

FIG. 12. Variation of CO desorption probability, p_3. O_2 can adsorb on any site pair and the base set of parameters was used except for the variation in p_3.

SEARCH FOR OPTIMAL SITE CONFIGURATIONS

One question that arises is what the optimal configuration of α and β sites on the surface is in order to obtain the highest rate-per-α-site or the highest overall rate. One goal, after the correct mechanism is determined, would be the ability to design and prepare the optimal catalyst. Because of the low-temperature operating conditions associated with many of the applications of NMRO CO oxidation catalysts, an optimal but thermodynamically unstable site configuration may be kinetically stable over operating periods of practical length.

One possible way to search for the optimal surface configuration for a given set of rules and parameters would be to take an active site configuration found from a run with a random surface and propagate it periodically across a larger surface. During each run the cumulative number of reaction events occurring on each site was recorded after the start-up transient. This allowed us to look at each surface configuration, search for the most active α site, for example, and then examine the site configuration surrounding this site. We found that the most active site configurations changed as the rules for O_2 adsorption changed. Figure 13 shows several most-active site configurations at various fraction-β for cases in which O_2 can adsorb on any site pair and diagonal actions are allowed. Similar configurations and rates are obtained when diagonal actions are not allowed. For each configuration, the most active α site is the central site in the surrounding 7×7 site array shown. Note that the local α–β ratio and the rate on the most active α site are roughly constant even though the average α–β ratio and the average rate change substantially between different sets of patterns. Three of the five patterns shown have a local fraction-β in the 3×3 array of sites centered on the most active α site = 0.44 (4/9), one pattern has a local fraction-β = 0.56 (5/9), and one has a local fraction-β = 0.33 (3/9).

Another approach to finding an optimal site configuration would involve "evolution" of a surface toward a more active configuration. Starting with a random surface of a desired fraction-β, for example, the computer program could switch one of the least active α sites to a β site and one of the least active β sites to an α site. If this "mutation" resulted in an increase in rate, it would be preserved and another mutation would be tried. If the mutation resulted in a decrease in rate, it would be reversed.

The approach we have pursued most extensively involves searching for optimal periodic configurations of α and β sites. First we specify the size of a square "base array." Second we choose a fixed number of α and β sites that will populate this base array. Third, the specified number of α and β sites are placed in the base array in one of the statistical combinations that are possible. Finally, the base array is propagated periodically and equally in two dimensions for a specified number of repetitions. The resulting square surface is specified to have the conventional periodic boundary conditions with respect to O_2 adsorption and surface reaction. Finally, the reaction is run on the resulting surface and a time-averaged steady-state rate is determined. Results for two of the cases we have studied are reported here: in one case diagonal actions were allowed, and in the other case diagonal actions were not allowed. In both cases O_2 adsorption can occur an any site pair and the base set of parameter values was used.

The smallest possible base array is a 1×1 array. The only configurations possible are the all-α surface and the all-β surface. These surfaces are also possible surfaces for all larger base arrays and will not be mentioned below. Both of these surfaces are inactive for the two cases considered here.

The next larger base array is a 2×2 array. Simulations were performed with surfaces in which the base arrays were propagated periodically eight times in both directions, with the entire 16×16 arrays having conventional periodic boundary conditions for reaction and O_2 adsorption. All surfaces

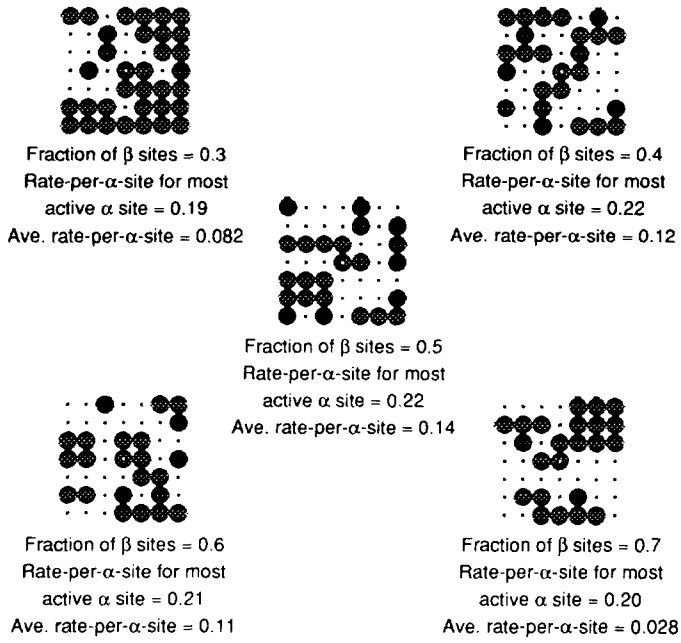

FIG. 13. Sections showing the site configurations surrounding the most active α sites present in individual random α–β surfaces for the case in which O_2 can adsorb on any site pair and for the base set of parameters. α sites are represented as large black circles and β sites are represented as small black dots, with adsorbed species not shown. The most active α site is the central site in each section and is marked with a white dot at its center. For this set of reaction rules and parameter values, the rate-per-α-site for the most active α sites in random surfaces is about 0.2 at all active fraction-β.

with 2×2 base arrays were inactive for the two cases considered here, with two exceptions. One exception is a 50–50 mixture of α and β sites arranged in alternating nondiagonal rows of α and β sites. This surface is active for the case considered in which diagonal actions are not allowed, and the rate-per-α-site is 0.06. The rate-per-α-site for a 50–50 mixture of α and β sites arranged randomly is 0.13.

The other exception is a 50–50 mixture of α and β sites arranged in alternating diagonal rows of α and β sites, a configuration which looks like a "checkerboard" of α and β sites. This surface is active for the case considered in which diagonal actions are allowed, and the rate-per-α-site is 0.17, higher than for the 50–50 random surface.

The c(2×2)–Sn/Pd(100) surface alloys studied experimentally by Logan and Paffett (*42*) have a checkboard configuration of Pt and Sn atoms, as determined by low energy electron diffraction and surface composition measurements. They found that the surface was active for CO oxidation when exposed to 16-Torr CO and 8-Torr O_2 at 170°C, however, the checkerboard structure was disrupted as Sn became oxidized and presumably formed SnO_x patches on top of the surface. An interesting question is whether the checkerboard Pt–Sn surface alloy would be stable and have a high activity for CO oxidation under milder conditions than used in (*42*).

The next larger base array is a 3×3 array. This base array is sufficiently large that a large number of interesting surface configurations are possible. For each specified ratio of α and β sites, each distinct configuration of sites is a statistical "combination." A search of possible statistical combinations of α and β sites was performed in the follow-

ing manner in order to achieve a confidence limit of >99.9% of trying all nonequivalent combinations: A configuration in the base array which does not have two- or fourfold rotational symmetry is equivalent, with respect to reaction, to the three other distinct statistical combinations that are formed by rotation of this nonrotationally symmetric configuration. By running a number of trials with random generation of site configuration equal to twice the number of possible statistical combinations, at least one of these four equivalent configurations will be tried within a confidence limit of >99.9%. During the same number of trials, at least one of the four equivalent configurations of all combinations which do not have two- or fourfold rotational symmetry will also be tried within this confidence limit. Configurations in the square base arrays that have two- or fourfold rotational symmetry were run deliberately by specifying the site configurations manually in separate runs.

The search for optimal site configurations with 3 × 3 base arrays was performed with surfaces in which the base arrays were propagated periodically seven times in both directions, with the entire 21 × 21 arrays having conventional periodic boundary conditions for reaction and O_2 adsorption.

Figures 14 and 15 summarize the results of the searches performed with 3 × 3 base arrays. Figure 14 is for runs in which diagonal actions are not allowed and Fig. 15 is for runs in which diagonal actions are allowed. The notation below each pattern gives the fraction-β, the rate-per-α-site, and rate-per-α-site over a random surface with the same fraction-β. The effect of disallowing or allowing diagonal actions on the most active site configurations is clear: in Fig. 14 the α and β sites tend to be arranged in horizontal and vertical rows, whereas diagonal groupings of α sites and β–β site pairs are prevalent in Fig. 15. Note the similarity between the local configurations of the most active α sites in random surfaces, shown in Fig. 13, and the optimal 3 × 3 base-array configurations found for the same rules and parameters in Fig. 15, especially the lower left configuration.

For the case in which diagonal actions are not allowed, all of the patterns in Fig. 14 are more active than the checkerboard pattern, which is inactive. For the case in which diagonal actions are allowed, all of the patterns in Fig. 15 are less active than the checkerboard pattern.

In Fig. 15, one can form the optimal three-β-site pattern simply by adding one β site to the base array of the optimal two-β-site pattern. Adding one β site to the base array of the optimal three-β-site pattern forms the optimal four-β-site pattern, and so forth to form the optimal five-β-site pattern. A similar progression can be done in Fig. 14, except that movement of a β site is required to go from the optimal three-β-site pattern to the optimal four-β-site pattern.

The results of Fig. 3 for random surfaces over which O_2 can adsorb on any site pair can be compared with the results of Fig. 15 for optimal 3 × 3 base-array patterns with the same O_2 adsorption rules. In most cases in which the 3 × 3 patterns are active, they are somewhat more active than a random surface at the same fraction-β. The 3 × 3 patterns are inactive below fraction-β = 0.22 and above fraction-β = 0.56, whereas random surfaces are active except at fraction-β = 0 and at fraction-β = 0.8 and above.

The rate-per-α-site of the most active α site was about 0.2 reaction events per CO collision for all random surfaces corresponding to the diagonal-pair rules and fraction-β shown in Figs. 14 and 15. This rate is higher than the rates found for the checkerboard pattern and the patterns in the 3 × 3 search. This suggests that a base array larger than the 3 × 3 base array may be required in order to construct the overall optimal pattern of α and β sites.

The next larger base array is the 4 × 4 base array. We did not do a complete study of 4 × 4 base arrays since the number of possible configurations is very large. From observing the patterns found in the 3 × 3

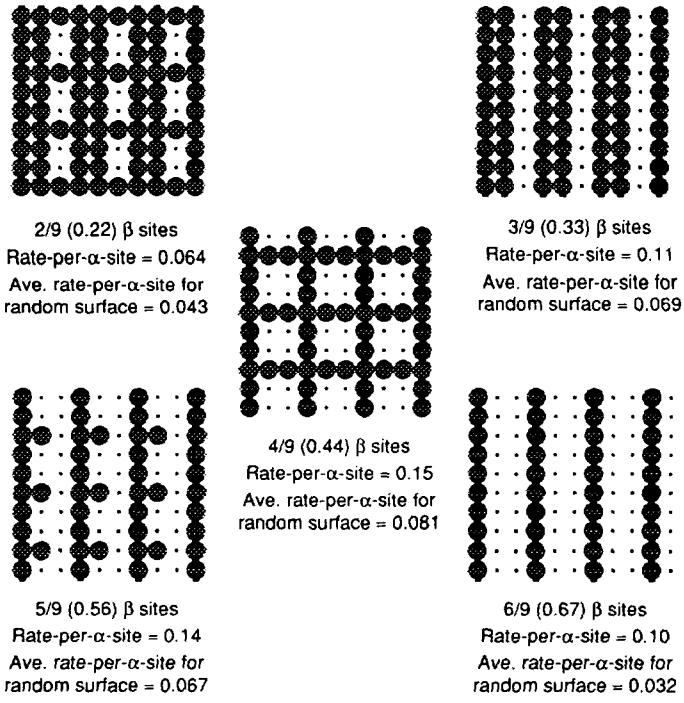

FIG. 14. The most active configurations found for 3 × 3 base arrays for cases in which diagonal actions are not allowed. O_2 can adsorb on any nondiagonal site pair, and the base set of parameters was used with the exception of not allowing diagonal actions. α sites are represented as large black circles and β sites are represented as small black dots. The case in which there is one β site in the nine-site base array is inactive due to CO poisoning, and the cases in which there are seven or eight β sites in the base array are inactive due to oxygen poisoning of the α sites.

base array search, we inferred that the 4 × 4 base-array configuration shown in the upper right quadrant of Fig. 16 would have high activity for the case in which diagonal actions are allowed. The rate-per-α-site over this "zig-zag" pattern is higher than any found in the 3 × 3 base array search but is 4% less than over the checkerboard pattern shown in the upper left quadrant of Fig. 16. The zig-zag pattern is probably less active than the checkerboard because an oxygen atom adsorbed on an α site can be removed by CO molecules adsorbed on other α sites along only one diagonal direction (i.e., the α chains are isolated from each other), and a buildup of adsorbed oxygen atoms in one section of an α chain can lead to deactivation of this section of the chain. In the checkerboard, an oxygen atom adsorbed on an α site can be removed by CO molecules adsorbed on other α sites along two diagonal directions.

Adding one α site to the 4 × 4 base array that forms the zig-zag pattern produces the "zig-zag + 1α" pattern shown in the lower right quadrant of the figure. This pattern has a lower rate-per-α-site than the pattern above it but has the highest overall rate of any surface we have identified. Note that the zig-zag chains of α sites in the zig-zag + 1α pattern are connected to each other at points every four α's along the chains, thus reducing the chance that a section of α chain will be deactivated by adsorbed oxygen. The "checkerboard + 1α" pattern, formed by adding one α site to the 4 × 4 base array that forms the checkerboard pattern, is 0.2% less active than the zig-zag +

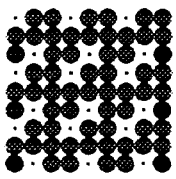

2/9 (0.22) β sites
Rate-per-α-site = 0.044
Ave. rate-per-α-site for random surface = 0.050

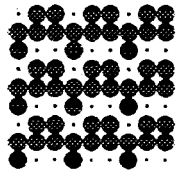

3/9 (0.33) β sites
Rate-per-α-site = 0.12
Ave. rate-per-α-site for random surface = 0.098

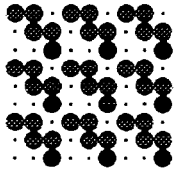

4/9 (0.44) β sites
Rate-per-α-site = 0.16
Ave. rate-per-α-site for random surface = 0.13

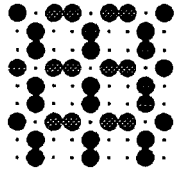

5/9 (0.56) β sites
Rate-per-α-site = 0.13
Ave. rate-per-α-site for random surface = 0.12

FIG. 15. The most active configurations found for 3 × 3 base arrays for cases in which diagonal actions are allowed. O_2 can adsorb on any site pair, and the base set of parameters was used. α sites are represented as large black circles and β sites are represented as small black dots. The case in which there is one β site in the nine-site base array is inactive due to CO poisoning, and the cases in which there are six, seven, or eight β sites in the base array are inactive due to oxygen poisoning of the α sites.

1α pattern. Subtracting one α site from the 4 × 4 base arrays of the two top patterns in the figure results in decreases in both the rates-per-α-site and the overall rates.

SUMMARY

This study demonstrates how high activity for CO oxidation can be obtained over a composite material composed of a highly interspersed mixture of one type of site, α, that adsorbs CO and O_2 and another type of site, β, that adsorbs O_2 without significant CO inhibition. As long as O_2 can adsorb on a pair of β sites, this mode of O_2 adsorption will predominate at low temperatures, where the CO desorption probability is low, over other possible modes of O_2 adsorption. The main effect of O_2 adsorption on α–α or α–β pairs is partial deactivation of the surface at high fraction-β, and this deactivation will be minimal when the O_2 sticking probability on α sites is low relative to the CO sticking probability, except at extremely high fraction-β. For some reaction rules and parameter values, specific α–β ratios or specific site configurations are inactive. For most reaction rules and parameter values, a roughly 50–50 mixture of the two types of sites will give the greatest activity per unit total surface area. This result is determined

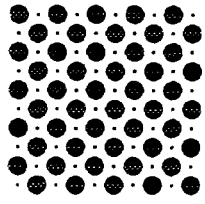

checkerboard

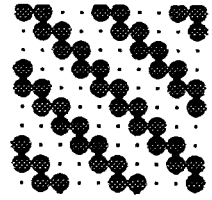

zig-zag

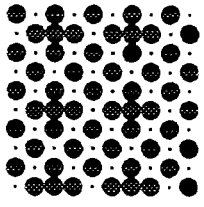

checkerboard + 1α

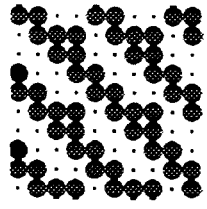

zig-zag + 1α

FIG. 16. 4 × 4 base-array patterns with high activity for the case in which O_2 can adsorb on any site pair, diagonal actions are allowed, and the base set of parameters is used. The two top patterns are composed of 8/16 (0.5) β sites. The checkerboard pattern (also a 2 × 2 base-array pattern) has the highest rate-per-α-site, 0.174, of any pattern studied in this work. The zig-zag pattern has a rate-per-α-site of 0.167. Random surfaces with this fraction of β sites have an average rate-per-α-site of 0.13. The overall rates for the checkerboard, zig-zag, and random patterns are 0.087, 0.084, and 0.065, respectively. The two bottom patterns are composed of 7/16 (0.44) β sites. The two bottom patterns have lower rates-per-α-site but higher overall rates than the two top patterns. The rates-per-α-site for the checkerboard + 1α, the zig-zag + 1α, and random patterns with the same fraction-β are 0.1575, 0.1580, and 0.13, respectively. The overall rates for the checkerboard + 1α, the zig-zag + 1α, and random patterns with the same fraction-β are 0.08857, 0.08875, and 0.073, respectively. The zig-zag + 1α pattern has the highest overall rate of any pattern studied in this work.

by the reaction stoichiometry and the fact that the two reactants primarily adsorb separately on the two different types of sites.

The sites in a randomly distributed mixture of the two types of sites have widely differing activities which depend on the local site configurations. The local site configurations of the most active sites in a random surface are similar to site configurations found in the search for optimal configurations. The site configurations found in the search for optimal configurations were only about 20% more active than the random surfaces of the same overall composition. This small difference may be due to the relatively simple steric requirements of CO and O_2 adsorption. We expect that similar searches for optimal site configurations will be more fruitful for reactions with more complex steric requirements.

More detailed experimental studies of reaction kinetics over composite catalysts are required in order to advance our understanding of low-temperature CO oxidation. The present work emphasizes the need for measurements of surface composition and surface structure. The use of scanning nanoprobe techniques with model catalyst systems, such as Pd–Sn surface alloys (*42*), should be especially useful. One particularly interesting question is what the relative contributions are of (a) enhanced reaction at the perimeter of noble-metal particles, predicted by the simulations of Brosilow *et al.* (*9*) and (b) reaction over highly interspersed mixtures of the two components, the presence of which have been identified experimentally by Hoflund and co-workers (*39, 40*) and the kinetics of which have been simulated in this work.

ACKNOWLEDGMENT

Work at the University of California, San Diego, was supported by NASA Grant 1-1051.

REFERENCES

1. Badlani, A., M.S. Thesis, Univ. Calif., San Diego, California, 1991.
2. Noordally, E., and Richmond, J. R., *in* "Low-Temperature CO-Oxidation Catalysts for Long-Life CO_2 Lasers, NASA Conf. Publ. 3076" (D. R. Schryer and G. B. Hoflund, Eds.), pp. 387–402. National Information Service, Springfield, Virginia, 1990.
3. Oh, S. H., Bissett, E. J., and Battiston, P. A., "Mathematical Modeling of Electrically Heated Monolith Catalytic Converters." Presented to American Chemical Society, April 1992.
4. Stark, D. S., and Harris, M. R., *J. Phys. E* **16,** 492 (1983).
5. Smith, A. L. S., Sephton, J. P., and Scott, G., *J. Phys. E* **17,** 590 (1984).
6. Poziomek, E. J., *in* "Low-Temperature CO-Oxidation Catalysts for Long-Life CO_2 Lasers, NASA Conf. Publ. 3076" (D. R. Schryer and G. B. Hoflund, Eds.), pp. 403–409. National Information Service, Springfield, Virginia, 1990.
7. Engel, T., and Ertl, G., *Adv. Catal.* **28,** 1 (1979).
8. Ziff, R. M., Gulari, E., and Barshad, Y., *Phys. Rev. Lett.* **56,** 2553 (1986).
9. Brosilow, B. J., Gulari, E., and Ziff, R. M., *J. Chem. Phys.* **98,** 674 (1993).
10. Araya, P., Porod, W., Sant, R., and Wolf, E. E., *Surf. Sci.* **208,** L80–L90 (1989).
11. Silverberg, M., and Ben-Shaul, A., *J. Chem. Phys.* **87,** 3178 (1987).
12. Dumont, M., Poriaux, M., and Dagonnier, R., *Surf. Sci.* **169,** L307 (1986).
13. Dumont, M., and Dufour, P., *Comput. Phys. Commun.* **41,** 1 (1986).
14. Meakin, P., and Scalapino, D., *J. Chem. Phys.* **87,** 731 (1987).
15. Vlachos, D. G., Schmidt, L. D., and Aris, R., *Surf. Sci.* **249,** 248 (1991).
16. Mukesh, D., *J. Catal.* **133,** 153 (1992).
17. Ziff, R. M., and Brosilow, B. J., *Phys. Rev. A* **46,** 4630 (1992).
18. Dumont, M., Poriaux, M., and Dagonnier, R., *Surf. Sci.* **169,** L307 (1986).
19. Chopard, B., and Droz, M., *J. Phys. A* **21,** 205 (1988).
20. Schwanker, R., Eiswirth, M., Moller, P., Wetzel, K., and Ertl, G., *J. Chem. Phys.* **87,** 742 (1987).
21. Moller, P., Wetzel, K., Eiswirth, M., and Ertl, G., *J. Chem. Phys.* **85,** 5328 (1986).
22. Wicke, E., Kummann, P., Keil, W., and Schiefler, J., *Ber. Bunsenges. Phys. Chem.* **84,** 315 (1980).
23. Lindenberg, K., West, B. J., and Kopelman, R., *Phys. Rev. Lett.* **60,** 1777 (1988).
24. Kopelman, R., *Science* **241,** 1620 (1988).
25. Ziff, R. M., and Fichthorn, K., *Phys. Rev. B* **34,** 2038 (1986).
26. Fichthorn, K., Gulari, E., and Ziff, R., *Phys. Rev. Lett.* **63,** 1527 (1989).
27. Fichthorn, K. A., Ziff, R. M., and Gulari, E., *Stud. Surf. Sci. Catal.* **38,** 883 (1987).
28. Fichthorn, K., Gulari, E., and Ziff, R., *Chem. Eng. Sci.* **44,** 1403 (1989).

29. Silverberg, M., and Ben-Shaul, A., *J. Chem. Phys.* **83,** 6501 (1985).
30. Silverberg, M., and Ben-Shaul, A., *J. Chem. Phys.* **87,** 3178 (1987).
31. Herz, R. K., *in* "Closed-Cycle, Frequency-Stable CO_2 Laser Technology, NASA Conf. Publ. 2456" (C. E. Batten, I. M. Miller, G. M. Wood, Jr., and D. V. Willetts, Eds.), pp. 103–112. National Information Service, Springfield, Virginia, 1987.
32. Herz, R. K., *in* "Low-Temperature CO-Oxidation Catalysts for Long-Life CO_2 Lasers, NASA Conf. Publ. 3076" (D. R. Schryer and G. B. Hoflund, Eds.), pp. 21–40. National Information Service, Springfield, Virginia, 1990.
33. Gardner, S. D., and Hoflund, G. B., *in* "Low-Temperature CO-Oxidation Catalysts for Long-Life CO_2 Lasers, NASA Conf. Publ. 3076" (D. R. Schryer and G. B. Hoflund, Eds.), pp. 123–138. National Information Service, Springfield, Virginia, 1990.
34. Haruta, M., Yamada, N., Kobayashi, T., and Iijima, S., *J. Catal.* **115,** 301 (1989).
35. Bond, G. C., Fuller, M. J., and Molloy, L. R., *in* "Proceedings, 6th International Congress on Catalysis, London, 1976" (G. C. Bond, P. B. Wells, and F. C. Tompkins, Eds.), pp. I:356–364. The Chemical Society, London, 1977.
36. Bond, G. C., Molloy, L. R., and Fuller, M. J., *J. Chem. Soc. Chem. Commun.* **19,** 796 (1975).
37. Brittan, M. I., Bliss, H., and Walker, C. A., *AIChE J.* **16,** 305 (1970).
38. Schryer, D. R., Upchurch, B. T., Sidney, B. D., Brown, K. G., Hoflund, G. B., and Herz, R. K., *J. Catal.* **130,** 314 (1991).
39. Gardner, S. D., Hoflund, G. B., Davidson, M. R., and Schryer, D. R., *J. Catal.* **115,** 132 (1989).
40. Drawdy, G. E., Hoflund, G. B., Gardner, S. D., Yngvadottir, E., and Schryer, D. R., *in* "Low-Temperature CO-Oxidation Catalysts for Long-Life CO_2 Lasers, NASA Conf. Publ. 3076" (D. R. Schryer and G. B. Hoflund, Eds.), pp. 201–207. National Information Service, Springfield, Virginia, 1990.
41. Oh, S. H., and Carpenter, J. E., *J. Catal.* **98,** 178 (1986).
42. Logan, A. D., and Paffett, M. T., *J. Catal.* **133,** 179 (1992).
43. Vannice, M. A., and Sudhakar, C., *J. Phys. Chem.* **88,** 2429 (1984).
44. Hoflund, G. B., Grogan, A. L., Jr., and Asbury, D. A., *J. Catal.* **109,** 226 (1988).
45. Vlachos, D. G., Schmidt, L. D., and Aris, R., *J. Chem. Phys.* **93,** 8306 (1990).
46. Falconer, J. L., and Schwarz, J. A., *Catal. Rev.-Sci. Eng.* **25,** 141 (1983).
47. Mundschau, M., and Rausenberger, B., *Platinum Met. Rev.* **35,** 188 (1991).
48. Upchurch, B. T., Kielin, E. J., and Miller, E. M., *in* "Low-Temperature CO-Oxidation Catalysts for Long-Life CO_2 Lasers, NASA Conf. Publ. 3076" (D. R. Schryer and G. B. Hoflund, Eds.), pp. 69–90. National Information Service, Springfield, Virginia, 1990.
49. Brosilow, B. J., and Ziff, R. M., *Phys. Rev. A,* **46,** 4534 (1992).
50. Gland, J. L., Sexton, B. A., and Fisher, G. B., *Surf. Sci.* **95,** 587 (1980).
51. Sampson, C. F., and Gudde, N. J., *in* "Closed-Cycle, Frequency-Stable CO_2 Laser Technology, NASA Conf. Publ. 2456" (C. E. Batten, I. M. Miller, G. M. Wood, Jr., and D. V. Willetts, Eds.), pp. 65–76. National Information Service, Springfield, Virginia, 1987.